Reconstruction with most likely trajectory for proton computed tomography

Tianfang Li* and Jerome Liang
Department of Radiology, State University of New York, Stony Brook, NY 11794, USA

ABSTRACT

Advantages of proton computed tomography (pCT) have been recognized in the past decades. However, the quality of pCT images is limited due to the stochastic nature of the proton path inside the object. Numerous small angle scatters by the nuclei Coulomb field cause the exact proton path impossible to trace. The reconstruction from measurements of the proton energy-loss has a spatial resolution limit due to these deflections. However, it has been shown that the proton path inside a uniform medium follows certain probability distribution so that a most likely trajectory (MLT) can be derived analytically for each proton. For real scan of a regular non-uniform object in pCT, the internal trajectory is better approximated by the MLT rather than a straight-line estimation. In this report, we presented preliminary studies on how the curved trajectories would affect the quality of the reconstructed images, and how much improvement we can achieve in reconstruction with the exact trajectory information. Analytical simulations with three phantoms, including a uniform disk phantom, multi-hole Aluminum phantom and Shepp-Logan phantom, were performed using artificial internal trajectories calculated based on the entrance and exit proton information. Reconstructions with the exact paths were compared to those with the straight-line path estimation. Significant improvement in density uniformity and spatial resolution were observed in the reconstructions with the path information.

Keywords: Proton CT, most likely trajectory, ART and FBP algorithms, multiple scattering.

1. INTRODUCTION

Proton computed tomography (pCT) has two major possible advantages in medical applications. First for diagnosis, its low-dose advantage might be utilized effectively to provide CT image reconstruction with significantly better density contrast resolution than conventional x-ray CT (xCT) at a given dose level. Its unique imaging characteristics based on linear stopping power of charged particles, as compared to the x-ray attenuation coefficient, may prove beneficial in medical diagnosis. Secondly, a successful implementation of pCT would avoid or simplify many of the current tedious procedures for proton therapy, including xCT imaging, mapping of xCT numbers to proton stopping power values, moving and repositioning the patient, and patient position-checking in the treatment room [1, 2].

A conceptual pCT system, which is similar to the first generation of xCT, is illustrated in Fig. 1. The data scanning is accomplished by translation and rotation operations. Instead of x-rays (portion of which is absorbed in the body), pCT utilizes a high energy (100-250 MeV) proton beam, all of which penetrate through the body.

One merit of proton imaging techniques is that the particles can be detected one-by-one, avoiding the quantum noise of xCT imaging. With present technologies, both the location and direction of each entrance and exit proton can be recorded as well as the energy of each exit proton, while the entrance energy is presumed to be known with excellent accuracy. This provides more information than xCT, and may be beneficial for image reconstruction.

The major difficulty of pCT imaging comes from the stochastic path of the particles inside the body. Numerous small angle deflections by the nuclei Coulomb field of the body make the estimation of the proton path very challenging. Therefore, the reconstruction of pCT from measurement of proton energy loss encounters a resolution limit due to these deflections. However, it has been shown that the proton path inside a uniform media follows certain probability distribution so that a most likely trajectory can be derived analytically [3,4]. In this work, we studied how

* tfli@mil.sunysb.edu; phone 1 631 444-7999; fax 1 631 444-6450

Medical Imaging 2004: Image Processing, edited by J. Michael Fitzpatrick, Milan Sonka, Proceedings of SPIE Vol. 5370 (SPIE, Bellingham, WA, 2004)
1605-7422/04/$15 doi: 10.1117/12.535811

these curved trajectories would affect the resolution of the reconstructed images, and how much improvement we can achieve in reconstruction with the exact trajectory information.

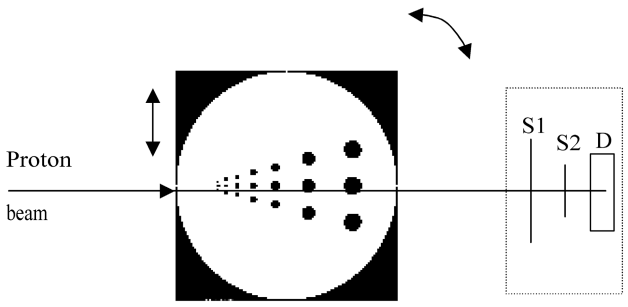

Fig. 1. Schematic diagram of a conceptual pCT system. The proton pencil beam and detectors remain stationary while the object moves and rotates. The detection part includes two position sensitive silicon detectors (S1 and S2), and a scintillation detector (D) to measure the residual proton energy.

2. BACKGROUND THEORIES

2.1 Principle of proton CT

The main principle of pCT is based on the determination of the integrated volume electron density, ρ_e, by measuring the energy loss of protons after traversing through the image object. The volume electron density of a medium is defined as the number of electrons/cm^3. The relationship between volume electron density and physical density is given by

$$\rho_e = \rho N_A \left(\frac{Z}{A} \right) \tag{1}$$

where ρ is the physical density, N_A is Avogadro's number (6.023×10^{23}), and Z and A are the (effective) atomic number and atomic weight of the traversed material, respectively. Since the ratio Z/A is fairly constant for human tissues, the electron density closely reflects the physical density of the imaged tissues. To avoid the large numbers associated with absolute volume electron density values (which are of the order of 10^{23} electrons/cm^3), it is better to express results in terms of relative volume electron density, which is defined as

$$\eta_e = \frac{\rho_e}{\rho_{e,water}} \tag{2}$$

where $\rho_{e,water} = 3.343 \times 10^{23}$ electrons/cm^3 is the volume electron density of water.

Ionization and atomic excitation mainly govern the energy loss of protons, and its mean rate (or stopping power) is given by the Bethe-Bloch equation,

$$-\frac{dE}{dx}(\mathbf{r}) = \eta_e(\mathbf{r})\, F(I(\mathbf{r}), E(\mathbf{r})) \tag{3}$$

where $\mathbf{r}$ represents the spatial location, $I(\mathbf{r})$ is the mean ionization potential of the medium, and $E(\mathbf{r})$ is the proton energy, which changes with $\mathbf{r}$ as the proton travels through the medium. Based on the Bethe Bloch equation, the function $F(I(\mathbf{r}), E(\mathbf{r}))$ can be expressed as[1]

[1] Note that the formula given here is an approximation of the original Bethe-Bloch equation, which contains a term W_{max}, the maximum energy transfer in a single collision. This approximation is valid if the mass of the incident projectile is large relative to the electron mass, which is the case for protons.

$$F(I(\mathbf{r}),E(\mathbf{r})) = K\frac{1}{\beta^2(E)}\left[\ln\left(\frac{2m_e c^2}{I(\mathbf{r})}\frac{\beta^2(E)}{1-\beta^2(E)}\right)-\beta^2(E)\right] \tag{4}$$

where $m_e c^2$ is the electron rest energy, and $\beta(E)$ is the proton velocity relative to c (the speed of light). The constant K is defined as

$$K = 4\pi r_e m_e c^2 \rho_{e,water} = 0.170\frac{\text{MeV}}{\text{cm}} \tag{5}$$

where r_e is the classical electron radius (2.818×10^{-13} cm). The relationship between β and E is given by

$$\beta(E) = \sqrt{1-\left(\frac{E_0}{E+E_0}\right)^2} \tag{6}$$

where E_0 = 938.27 MeV is the proton rest energy.

Note that the Bethe-Bloch equation (3) is a non-linear first-order differential equation of the function $E(\mathbf{r})$. Since $I(\mathbf{r})$ is usually not known in pCT, integration of this equation is not possible. However, for human tissues the variation of I is relatively small, and the dependence of the function F on I is relatively weak due to the logarithmic function. Therefore, it is reasonable to assume that $I(\mathbf{r})$ is independent of location and can be replaced by the mean ionization potential of water I_{water} = 61.77 eV. In this case, F is only a function of E and equation (3) can be integrated after separating variables:

$$\int_S \eta_e(\mathbf{r})dx = \int_{E_{out}}^{E_{in}} \frac{dE}{F(I_{water},E)} \tag{7}$$

where the integration on the left side is along the proton path S, and on the right side E_{in} is the incident proton energy and E_{out} is the proton energy after traversing the object. It is now obvious that the integrated relative volume electron density can be calculated based on the knowledge of in- and out-going proton energy. Due to the complicated energy dependence of F, the integration must be performed numerically. Also note that the integrated density along the proton trajectory is nothing else than the water-equivalent length of the proton track through the medium. Equation (7) is in the format of the Radon transform if the proton path S is treated as a straight line.

2.2 Most likely trajectory (MLT)

According to Fermi's theory [5] of the scattering process, Schneider and Pedroni derived a projected distribution function $f(t,x,\theta)$ using Gaussian approximation for small angles [3]

$$f(t,x,\theta)dxd\theta = \frac{1}{\pi\sqrt{D_0^t}}e^{(-A_0^t\theta^2+2B_0^t x\theta-C_0^t x^2)tD_0^t}dxd\theta \tag{8}$$

where $f(t,x,\theta)$ is the probability that a proton undergoing multiple scattering in a homogenous material of thickness $z = tR$ ($0<t<1$) along the z-axis will be emitted at a projected angle θ in the (x, z)-plane and at a projected displacement x at z, where R is the range of the protons in the material and t is the traversed thickness measured as a fraction of the initial range, see Fig. 2.

If the energy dependence is neglected, the coefficients A, B, C, D can be achieved by the following equations:

$$A_0^t = \frac{1}{3}\alpha t^3R^3,\ B_0^t = \frac{1}{2}\alpha t^2R^2,\ C_0^t = \alpha tR,\ D_0^t = \frac{1}{12}\alpha t^4R^4 \tag{9}$$

where α is a constant depending on both the proton energy and the material.

As shown in Fig. 2, the differential probability dP_{AC} to detect a proton inside a small given interval Δx_t around point C and with an angle θ_t is $dP_{AC} = f(t, x_t, \theta_t)d\theta_t\Delta x_t$. The differential probability for a proton to reach a given exit point D, when starting from point C with an angle θ_t is $dP_{CD} = f(1\text{-}t, x_D\text{-}x_E, \theta_D\text{-}\theta_t)d\theta_t\Delta x_t$. Therefore, the probability that a

proton entering at A and exiting at D will pass through C is $dP_{ACD} = dP_{AC}*dP_{CD}$. The most probable trajectory maximizes the likelihood which is the integration over all possible angle θ_t, hence

$$\frac{\partial}{\partial x_t}\left(\int dP_{ACD}\ d\theta_t\right) = 0\ . \tag{10}$$

Finally we can get the following quite simple trajectory equation:

$$x_t = (3t^2 - 2t^3)x_D - (t^2 - t^3)R\theta_D\ , \tag{11}$$

where x_D and θ_D are the displacement along x-axis and the deflection angle of the detected proton, respectively. In Fig. 3 we showed several calculated MLTs given different possible x-displacements and deflection angles corresponding to the same entrance proton.

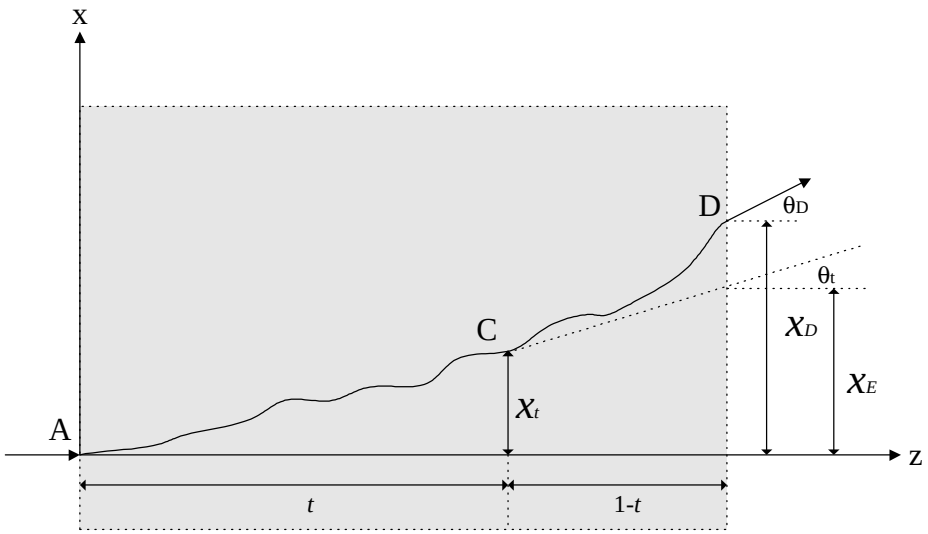

Fig. 2. Illustration of the calculation of the sidewise distribution of protons passing through two points A and D.

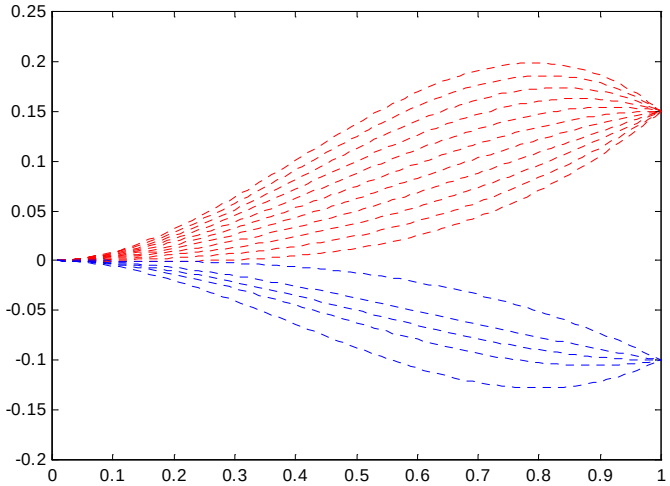

Fig. 3. Most likely trajectories calculated by equation (11) with different displacement and deflection angle settings.

3. ANALYTICAL DATA SIMULATIONS AND IMAGE RECONSTRUCTIONS

To study the impact of the curved internal paths on the reconstruction for pCT, we analytically simulated sinograms with the MLTs, and compared the reconstruction results with and without the path information. First, the *pseudo detections* were generated using Gaussian random number which represents the exit information that a real pCT detector would detect, *i.e.*, the information of the displacements and deflection angles. For example, if a proton entering at $x=x_0$, then the displacement of the exiting position will follow a Gaussian distribution $x_D \sim N(0,\sigma_x)$, and the deflection angle also follows a Gaussian distribution $\theta_D \sim N(\mu_\theta, \sigma_\theta)$. The deflection angle and the displacement along x-axis are strongly correlated, which is modeled here as $\sigma_x = \frac{1}{\sqrt{3}} t\sigma_\theta$. Based on the "detected" exit protons and equation (4), the corresponding internal MLTs can be calculated and used for simulating the pCT projections by curve integral.

Then the simulated projections were reconstructed with (i) the conventional FBP (filtered backprojection) method using straight-line path estimation, given the entrance and exit position; (ii) the simultaneous ART (algebraic reconstruction technique) method using the MLT information.

3.1 Uniformity test

MLTs were analytically calculated by equation (4), given the entrance and exit information of each proton randomly generated by Gaussian distributions. A total of 128 scan angles were simulated, each contains 128 proton trajectories. Fig. 4(a) illustrates one projection view of such proton trajectories; Fig. 4(b) is a uniform disk phantom, and Fig. 4(c) is the simulated projection data. It can be seen that some of the proton trajectories may intersect with each other. Therefore, unlike the xCT, the projection data of pCT may be insufficient for accurate reconstruction in some regions, and can be redundant in other regions. Hence, a simple FBP strategy will lead to non-uniform reconstruction.

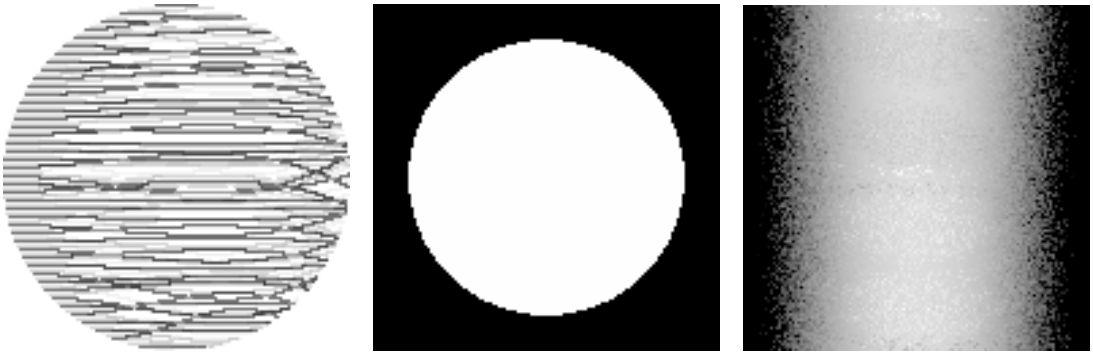

(a) (b) (c)

Fig. 4. (a) Randomly generated curved-trajectories, representing the MLTs of the protons inside an object. (b) A uniform disk phantom for simulation. (c) Simulated projection using (a) and (b).

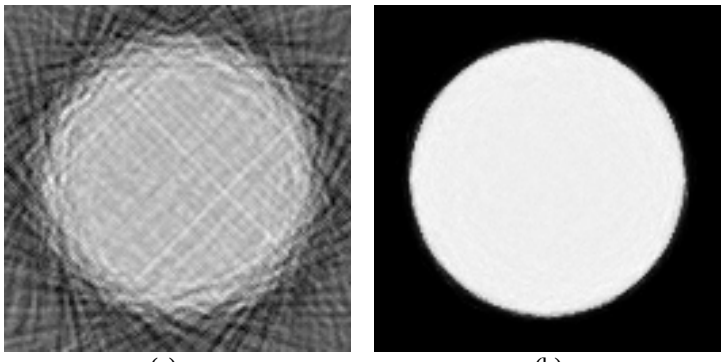

(a) (b)

Fig. 5. (a) FBP reconstructed image. (b) Simultaneous ART reconstruction for the same data.

It is expected that, without knowledge of the MLT's information, the conventional FBP reconstruction for strongly scattered proton CT gives a lower image quality for the simple uniform disk phantom experiment. Non-uniform density artifacts are presented from the center to the boundary in the reconstructed image, see Fig. 5(a). However, if we know all proton paths, as the case in this simulation study, the density uniformity can be improved dramatically by ART reconstruction method as shown in Fig. 5(b). The profiles along the central horizontal line were presented in Fig. 6 for the reconstructed images by the two methods, together with the profile of the phantom.

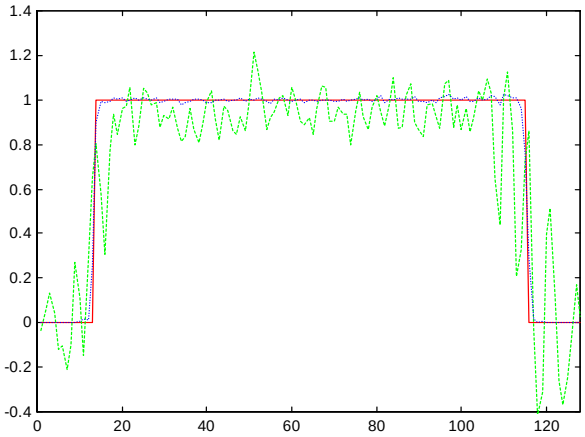

Fig. 6. Profile along the central horizontal line. The solid line is for the uniform disk phantom, the dotted line is for the ART reconstructed image with MLTs information (Fig. 5b), and the dash line is for the FBP reconstructed image (Fig. 5a).

3.2 Resolution test

In this experiment, the same proton paths were used to simulate the projection data from two other phantoms. One is a multi-hole Aluminum disk phantom, the other is the Shepp-Logan phantom, as shown in Figs. 7(a) and 7(b).

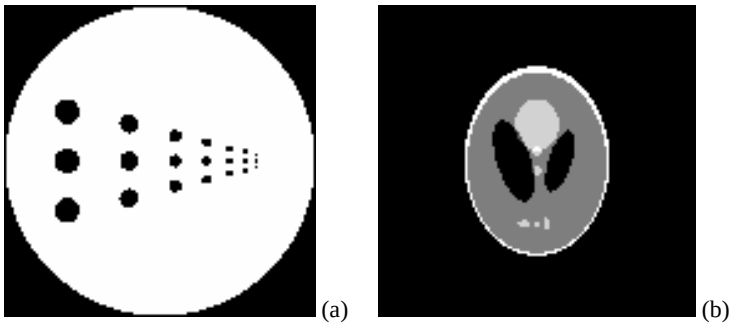
(a) (b)

Fig. 7. Two phantoms in simulation study. (a) is a multi-hole Aluminum disk phantom, and (b) is the Shepp-Logan phantom.

To demonstrate the impact of the random curved paths on the projection image, we presented the simulated pCT and xCT projection of the multi-hole Aluminum disk phantom in Fig. 8. The sinogram of pCT looks noisy due to the randomness of the projection paths (while xCT uses straight lines). The reconstructed images from the pCT sinogram by FBP (with straight lines) and ART (with curved paths) were compared in Fig. 9. It is clearly seen that most of the small holes were resolved in the ART reconstructed image, while the FBP image has very poor resolution with distortion.

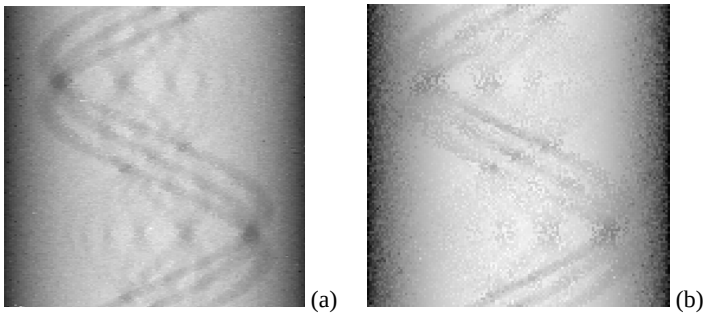

(a) (b)

Fig. 8. Simulated sinograms for xCT (a) and pCT (b).

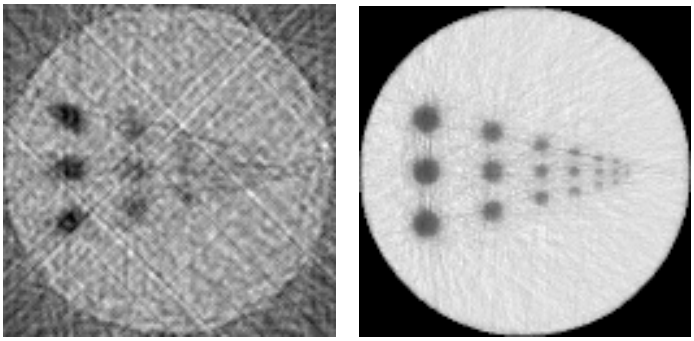

(a) (b)

Fig. 9. (a) FBP reconstruction for simulated pCT sinogram (Fig. 8b). (b) ART reconstruction with MLTs information for the same sinogram.

The experiment was repeated for the Shepp-Logan phantom, and the results were shown in Fig. 10. Given the internal trajectories of the sonogram (a), the reconstruction resolution (Fig. 10c) can be greatly improved from the conventional FBP using straight-line approximation (Fig. 10b).

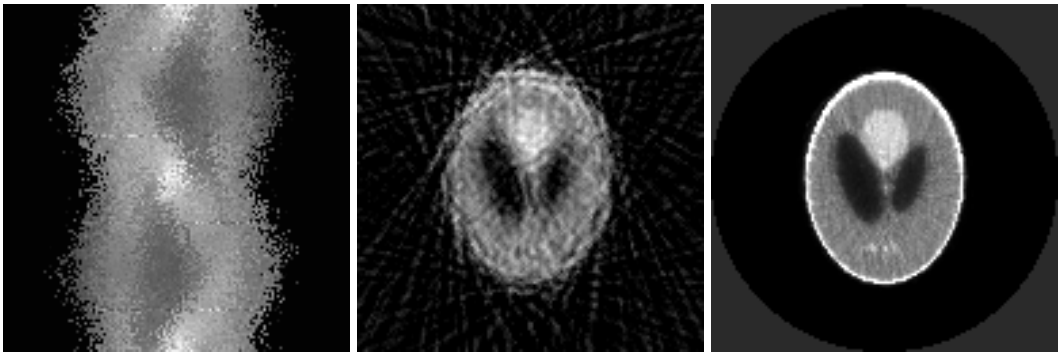

(a) (b) (c)

Fig. 10. (a) Analytical simulation of pCT sinogram using the Shepp-Logan phantom. (b) FBP reconstruction from sinogram (a). (c) Simultaneous ART reconstruction using MLTs from data (a).

4. CONCLUSIONS

The stochastic path of a charged particle inside the body limits the image quality and hence the use of pCT. To date, no algorithm has been developed to improve the reconstruction using the curved trajectory. In this report, we presented a pilot study to show the possibility that the MLT path estimation can significantly improve the image quality in pCT. In order to demonstrate this, we analytically simulated the pCT projections with three different phantoms, and compared the reconstructions with and without the exact internal trajectory information. The preliminary results showed that the

reconstruction with MLT could dramatically improve the image uniformity and spatial resolution. In a real pCT system, however, the exact proton path is not available and, therefore, the MLT can be an optimal choice to approximate the path which is more accurate than the straight line estimation. Since analytical (or non-iterative) FBP-type reconstruction for curved paths is not currently available, the ART (iterative) method was employed. Other iterative means can also be applied to this pCT reconstruction.

In this work, the MLT calculation by equation (4) is based on two assumptions, one is the constant energy of the proton beam, and the other is the uniform density of the target. Since the protons will loss energy while traveling inside the body, more accurate MLT estimation with energy dependence should be considered. Algorithms simultaneously segment and reconstruct the object may also be helpful to deal with the uniform density assumption [6, 7].

The chosen ART iterative method in this work utilizes the full knowledge of the exact path information by the simulation. In real word, however, the exact path is unknown, and can only be estimated, given the measurements. If the path probability distribution can be estimated given the entrance and exiting positions as well as the energy and other measurements, then the sinogram can be determined by tracing each proton through the body with the weights by the path probability distribution, rather than along a MLP curve. Tracing the path probability is very similar to tracing the collimator response kernel in SPECT (single photon emission computed tomography) [8].

An exact reconstruction method can be established to estimate both the path and the image density by an interleaved iterative manner, given the current iterated estimates of the path and the density. For example, we can update the path estimation to next iteration from current iterated path and image density. Then we can update the image density to next iteration from the updated path and the current iteration image density. This exact reconstruction is expected to be time consuming. However, with computer technology advancement, the reconstruction time could be reduced for possible clinical applications.

ACKNOWLEDGEMENT

This work was supported in part by the NIH National Heart, Lung and Blood Institute under Grant No. HL54166 and the NIH National Cancer Institute under Grant No. CA82402.

REFERENCES

1. K. Hanson, J. Bradbury, T. Cannon, R. Hutson, D. Laubacher, R. Macek, M. Paciotti, and C. Taylor, “Computed tomography using proton energy loss”, *Phys. Med. Biology*, **26**: 965-983, 1981.
2. K. Hanson, J. Bradbury, R. Koeppe, R. Macek, D. Machen, R. Morgado, M. Paciotti, S. Sandford, and V. Steward, “Proton computed tomography of human specimens”, *Phys. Med. Biology*, **27**: 25-36, 1982.
3. U. Schneider and E. Pedroni, “Multiple Coulomb scattering and spatial resolution in proton radiography”, *Medical Physics*, **21**: 1657-1663, 1994.
4. D.C. Williams, “The most likely path of an energetic charged particle through a uniform medium”, preprint, 2003.
5. B. Rossi and K. Greisen, “Cosmic-ray theory”, *Rev. Mod. Physics*, **13**: 240-268, 1941.
6. Z. Liang, R. Jaszczak, E. Coleman, and V. Johnson, “Simultaneous reconstruction, segmentation, and edge enhancement of relatively piecewise continuous images with intensity-level information”, *Medical Physics*, vol.**18**: 394-401, 1991.
7. Z. Liang, R. Jaszczak, and E. Coleman, “On reconstruction and segmentation of piecewise continuous images”, in *Information Processing in Medical Imaging*, **12**: 94-104, 1991.
8. Z. Liang, T. Turkington, D. Gilland, R. Jaszczak, and E. Coleman, “Simultaneous compensation for attenuation, scatter, and detector response for SPECT reconstruction in three dimensions”, *Phys. Med. Biology*, **36**: 587-603, 1992.